

Towards scalable active steering protocols for genuinely entangled state manifolds

Samuel Morales,¹ Silvia Pappalardi,² and Reinhold Egger¹

¹*Institut für Theoretische Physik, Heinrich-Heine-Universität, D-40225 Düsseldorf, Germany*

²*Institut für Theoretische Physik, Universität zu Köln, Zùlpicher Straße 77, 50937 Cologne, Germany*

We introduce and analyze an active steering protocol designed to target multipartite entangled states. The protocol involves multiple qubits subjected to weak Bell pair measurements with active feedback, where the feedback operations are optimized to maximize the Quantum Fisher Information. Our scheme efficiently reaches a genuinely entangled one-parameter state manifold. Numerical simulations for systems with up to 20 qubits suggest that the protocol is scalable and allows high multipartite entanglement across the system.

Introduction.—Active steering protocols have recently attracted a lot of attention [1–8]. By a sequence of (weak) measurements, followed by feedback operations determined by the measurement outcomes, one may prepare, stabilize, or manipulate arbitrary quantum states. (Following Ref. [9], we use “steering” as proxy for “guiding” the system, which differs from “quantum steering” in quantum information theory [10].) Weak, i.e., almost non-invasive, measurements can be performed, for instance, by weakly coupling each system qubit to its own detector qubit, with projective measurements of the detector qubits [11]. The feedback policy is typically based on a cost function. Previous active steering protocols, see, e.g., Refs. [4, 6, 8], have been limited to $N \leq 6$ system qubits, mainly because practically useful fidelity-based cost functions imply an exponential scaling of the algorithmic demands with system size (N).

In this work, we present an active steering protocol that utilizes the *Quantum Fisher Information* (QFI) [12] as a cost function. The QFI is a fundamental quantity in entanglement theory and quantum metrology, serving as a witness of multipartite entanglement [13–15] and a valuable resource for quantum-enhanced metrology [16–20]. Our QFI-based protocol allows one to efficiently reach a one-parameter manifold of genuinely entangled N -qubit states which maximize the QFI, namely Green-Hornberger-Zeilinger (GHZ) states [21],

$$|\Psi\rangle = \frac{1}{\sqrt{2}} (|000\dots\rangle + e^{i\phi}|111\dots\rangle), \quad (1)$$

with an angular parameter ϕ . (For a system qubit with Pauli matrices $\sigma^{x,y,z}$, we use $\sigma^z|0\rangle = |0\rangle$ and $\sigma^z|1\rangle = -|1\rangle$.) By using the QFI as cost function, our protocol significantly accelerates the active steering process. It also allows one to target a specific state with a designated phase ϕ . Additionally, our findings suggest scalability with the system size N , offering promising potential for steering in larger quantum systems. We note that if one stops the protocol before the maximal value for the QFI has been reached, one may also access more general states beyond Eq. (1).

Below, we formulate the active steering protocol in a platform-independent manner. However, since weak

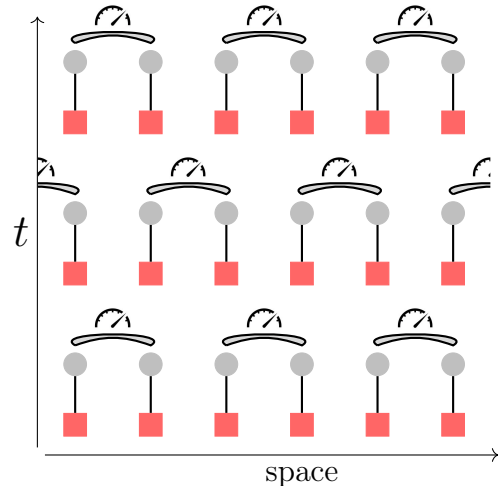


FIG. 1. Schematic time evolution of the active steering protocol. We show three time steps for $N = 6$ system qubits (red squares) coupled by steering operators H_n (straight vertical lines) to their own detector qubits (grey circles). The qubit chain has periodic boundary conditions. A possible scheme for the Bell measurements of neighboring detector qubit pairs in subsequent cycles is indicated.

measurements play a key role in the protocol, a physical realization with fast qubit readout is desirable, e.g., superconducting Andreev qubits with detector readout times of order 10 ns [22]. As shown in Ref. [8], active steering is robust against error channels with sufficiently weak error rate. For simplicity, we thus neglect external noise and study the idealized error-free case. Our protocol assumes that the system is initialized at time $t = 0$ in a simple product state, say, $|\Psi(t = 0)\rangle = |000\dots\rangle$, and that for a given measurement record, the state trajectory $|\Psi(t)\rangle$ can be stored and updated on a classical computer for each time step of the quantum protocol. In the conclusions, we briefly discuss how the state tracking requirement may be avoided altogether in modified versions of our scheme.

Protocol and QFI.—We schematically illustrate the protocol in Fig. 1. We consider N system qubits described by Pauli matrices σ_n^α (with $\alpha = x, y, z$ and $n = 1, \dots, N$), where each system qubit couples only to

its own detector qubit described by Pauli matrices τ_n^β . We neither allow for direct couplings between different system qubits nor between different detector qubits, while the Hamiltonian H_n (“steering operator”) for the n th system-detector qubit pair can be selected from the set of Pauli gates,

$$H_n = J\sigma_n^{\alpha_n}\tau_n^{\beta_n}, \quad (2)$$

with $\alpha_n \in \{x, y, z\}$ and $\beta_n \in \{x, z\}$. For simplicity, we assume a fixed coupling J and degenerate zero-energy states for all uncoupled qubits. The steering parameters $K_n = (\alpha_n, \beta_n)$ are chosen according to a decision making scheme in every time step of the protocol as described below, with $[H_n, H_{n'}] = 0$ for arbitrary K_n and $K_{n'}$.

The protocol starts at time $t = 0$ by initializing all system and detector qubits in $|0\rangle$ and $|0\rangle_d$ (the subscript d refers to detector qubit space), respectively, i.e., the system state is $|\Psi(t = 0)\rangle = |000\dots\rangle$. We then group the N qubits into neighboring pairs $(n, n + 1)$, see Fig. 1, where all subsequent operations for different pairs commute and can thus be performed simultaneously. (For odd N , one “idle” qubit remains whose location is chosen from a uniform random distribution.) Given the state $|\Psi(t)\rangle$, we select the steering couplings for this pair, (K_n, K_{n+1}) , such that the measurement-averaged expectation value of the QFI after a time step of duration δt is maximized.

For a pure N -qubit state $|\Psi\rangle$, the QFI is defined as [16–20]

$$F_Q = 4(\langle\Psi|\mathcal{O}^2|\Psi\rangle - \langle\Psi|\mathcal{O}|\Psi\rangle^2). \quad (3)$$

For collective observables $\mathcal{O} = \frac{1}{2}\sum_{n=1}^N O_n$, where O_n are local operators, the QFI can be used to probe the multipartite entanglement structure of the state $|\Psi\rangle$ [13–15]. If the QFI satisfies the inequality $F_Q > mN$, then at least $(m+1)$ parties of the system are entangled. Namely, $m \leq N$ represents the size of the biggest entangled block. The upper bound $F_Q \sim N^2$ corresponds to the so-called genuinely multipartite entanglement, and it is attained by the states in Eq. (1).

In our protocol, we parametrize $O_n = \mathbf{s}_n \cdot \boldsymbol{\sigma}_n$, with $\mathbf{s}_n = (s_n^x, s_n^y, s_n^z)$ an arbitrary unit vector and $\boldsymbol{\sigma}_n = (\sigma_n^x, \sigma_n^y, \sigma_n^z)$. Using the optimal choice for (K_n, K_{n+1}) , see the discussion after Eq. (6) below, one time-evolves the coupled system-plus-detector system for a time step δt . Next, a projective measurement of the detector qubit pair is done in its Bell basis $\{|\Phi_{\xi,\eta}\rangle_d\}$ [21], where $|\Phi_{\xi=0,\eta=\pm}\rangle_d = (|00\rangle_d \pm |11\rangle_d)/\sqrt{2}$ and $|\Phi_{\xi=1,\eta=\pm}\rangle_d = (|01\rangle_d \pm |10\rangle_d)/\sqrt{2}$. Symmetric ($\eta = +1$) and antisymmetric ($\eta = -1$) Bell states have even ($\xi = 0$) or odd ($\xi = 1$) parity, where “symmetry” refers to qubit exchange while even (odd) “parity” means that states are built from the basis $\{|00\rangle_d, |11\rangle_d\}$ ($\{|01\rangle_d, |10\rangle_d\}$). Such measurements can be implemented by commuting measurements of the Pauli operators $\tau_n^z \tau_{n+1}^z = \pm 1$ and

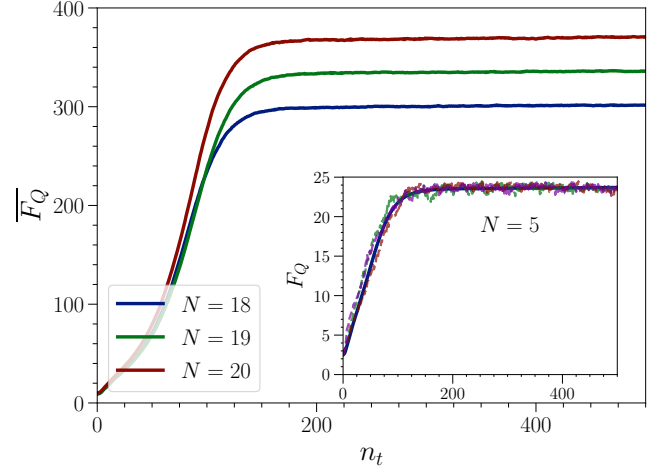


FIG. 2. Average QFI $\overline{F_Q}$ vs number of time steps $n_t = t/\delta t$ for different N and $J\delta t = 0.2$. Note that $F_Q \leq N^2$. Averages are over 100 trajectories. The inset shows $\overline{F_Q}$ vs n_t (solid curve) for $N = 5$ (averaged over 8000 trajectories), together with three individual measurement trajectories (dashed curves).

$\tau_n^x \tau_{n+1}^x = \pm 1$. Finally, one re-initializes all detector qubits in the state $|0\rangle_d$ and iterates the protocol until convergence has been achieved. Since the initial detector state $|00\rangle_d$ (for each time step and each qubit pair) has even parity, measurement outcomes with odd parity ($\xi = 1$) are referred to as quantum jumps. The above measurements realize entanglement swapping [23–30] and tend to increase entanglement in the system state $|\Psi(t)\rangle \rightarrow |\Psi(t + \delta t)\rangle$, see Ref. [6] for a detailed discussion.

In the weak measurement limit $J\delta t \ll 1$ [11], the state change $|d\Psi\rangle = |\Psi(t + \delta t)\rangle - |\Psi\rangle$ with $|\Psi\rangle = |\Psi(t)\rangle$ for measurement outcome (ξ, η) is governed by a jump-type nonlinear stochastic Schrödinger equation (SSE) [31–33],

$$|d\Psi\rangle = \left[-i\delta t H_0 + \xi \left(\frac{c_\eta}{\sqrt{\langle c_\eta^\dagger c_\eta \rangle}} - 1 \right) - \frac{\delta t}{2} (c_\eta^\dagger c_\eta - \langle c_\eta^\dagger c_\eta \rangle) \right] |\Psi\rangle, \quad (4)$$

where $H_0 = J\sum_{m=n,n+1} \delta_{\beta_m,z} \sigma_m^{\alpha_m}$ and $\langle c_\eta^\dagger c_\eta \rangle = \langle\Psi|c_\eta^\dagger c_\eta|\Psi\rangle$. The jump operators $c_{\eta=\pm}$ are given by

$$c_\eta = -iJ\sqrt{\delta t} (\eta\delta_{\beta_n,x}\sigma_n^{\alpha_n} + \delta_{\beta_{n+1},x}\sigma_{n+1}^{\alpha_{n+1}}), \quad (5)$$

where the outcome (ξ, η) has the *a priori* probability $p_{\xi,\eta} = \frac{1}{2}[\delta_{\xi,0} + (\delta_{\xi,1} - \delta_{\xi,0})\delta t \langle c_\eta^\dagger c_\eta \rangle]$. Averaging over the measurement outcomes after one time step, one arrives at the anticipated average change in QFI after the next

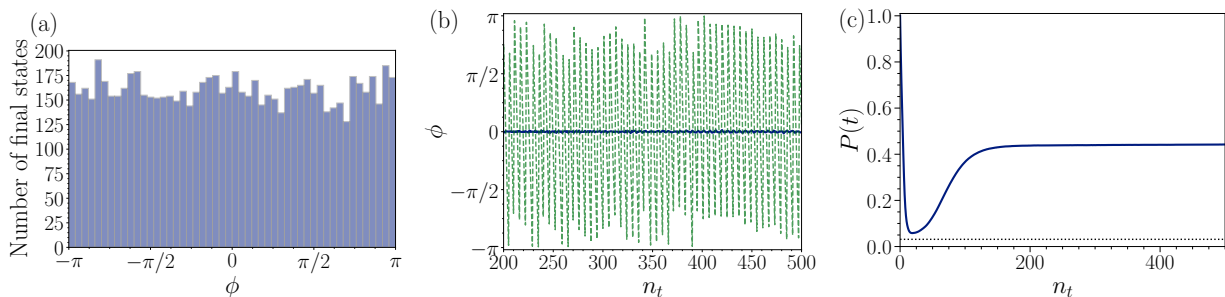


FIG. 3. Active steering protocol for $N = 5$ and $J\delta t = 0.2$. Measurement averages are over 8000 trajectories. (a) Histogram of the phase ϕ in Eq. (1) found after $n_t = 500$ time steps. (b) Time evolution of the phase ϕ after convergence to the target manifold has been reached, shown for one individual measurement trajectory (dashed green curve) and for the average (solid blue curve). (c) Purity $P(t)$ vs n_t , see Eq. (7). The dotted line corresponds to the maximally mixed (infinite temperature) state.

time step,

$$\begin{aligned} \langle dF_Q \rangle_{\text{ms}} &= \langle F_Q(t + \delta t) \rangle_{\text{ms}} - F_Q(t) \\ &= 4 \left(\text{tr}(\mathcal{O}^2 \langle d\rho \rangle_{\text{ms}}) - 2 \text{tr}(\mathcal{O} \langle d\rho \rangle_{\text{ms}}) \text{tr}(\mathcal{O}\rho) \right. \\ &\quad \left. - \langle [\text{tr}(\mathcal{O} d\rho)]^2 \rangle_{\text{ms}} \right) \end{aligned} \quad (6)$$

with $d\rho = |d\Psi\rangle\langle\Psi| + |\Psi\rangle\langle d\Psi| + |d\Psi\rangle\langle d\Psi|$ and $\rho = |\Psi\rangle\langle\Psi|$. (Here $\langle A \rangle_{\text{ms}}$ denotes a measurement average of the quantity A using the probabilities $p_{\xi,\eta}$.) For practical calculations, Eq. (6) is evaluated by using a Bloch tensor state representation [6]. We compute $\langle dF_Q \rangle_{\text{ms}}$ for all possible steering parameters and then choose (K_n, K_{n+1}) such that $\langle dF_Q \rangle_{\text{ms}}$ is maximized. In our numerical simulations, the system state is propagated according to the SSE (4). In contrast to Ref. [6], the time evolution is not terminated once a certain threshold value for F_Q has been reached but the quantum state trajectory continues evolving according to the above protocol.

Numerical simulation results.— We now show simulation results for the above protocol maximizing the QFI. For the steering operator set (2), it is convenient to choose $\mathbf{s}_n = \frac{1}{\sqrt{2}}(1, 0, 1)^T$, see Eq. (3), but our results are robust under small rotations of this unit vector. Correspondingly, the GHZ states (1) are defined with respect to rotated states $|0\rangle \rightarrow |0'\rangle$ and $|1\rangle \rightarrow |1'\rangle$. Up to a normalization factor, $|0'\rangle = |0\rangle + (\sqrt{2} - 1)|1\rangle$ and $|1'\rangle = (1 - \sqrt{2})|0\rangle + |1\rangle$. In Fig. 2, we show the evolution of the time-dependent QFI. The main panel illustrates the average QFI $\overline{F_Q(t)}$ (the overbar indicates an average over many measurement trajectories) for several values of N , where we observe that the QFI comes close to its maximum value $F_Q = N^2$ after $n_t \approx 200$ time steps. This number for n_t is basically independent of N . In the inset of Fig. 2, for $N = 5$, we illustrate the convergence behavior of the QFI both for individual measurement trajectories and for the average. Next we show that the target manifold (1) is reached to good accuracy. In Fig. 3(a), for $N = 5$, we show a histogram of

the phase $\phi = \arg(\langle 0'0'0' \dots | \Psi \rangle \langle \Psi | 1'1'1' \dots \rangle)$ measured after 500 time steps. We find that the histogram is rather flat, implying that the quantum state trajectories uniformly explore the entire manifold even though they all start from the same initial state. Alternatively, as illustrated in Fig. 3(b), one may take an individual measurement trajectory and follow it over time. For our choice of steering operators (2), almost regular oscillations are observed, where again all possible values of ϕ are reachable over the course of time. By invoking a termination policy, one can then target a specific state with a predesignated value of ϕ . We note that the oscillatory behavior appears to be linked to the specific sign choice of J in Eq. (2). Finally, in Fig. 3(c), we show the purity [34–36],

$$P(t) = \text{Tr}(\overline{\rho(t)}^2), \quad (7)$$

as a function of n_t . Interestingly, the average state $\overline{\rho(t)}$ first approaches an infinite-temperature state where the purity gap (almost) closes [37], but the purity then increases again towards the asymptotic value 1/2. This value is readily explained by the fact that averaging over the phase in Eq. (1), one produces the asymptotic average state

$$\bar{\rho} = \frac{1}{2} (|000 \dots\rangle\langle 000 \dots| + |111 \dots\rangle\langle 111 \dots|), \quad (8)$$

which has purity $P = 1/2$ for all N . The difference to the numerically observed asymptotic purity in Fig. 3(c) is due to the finite value of $J\delta t$. We find that this difference becomes smaller by reducing $J\delta t$, see also below.

Let us now discuss the dependences on the protocol's parameters. The scaling of the accuracy of the value of $\overline{F_Q}$ reached after $n_t = 500$ steps with system size N is shown in Fig. 4 for two values of $J\delta t$. We observe that for smaller $J\delta t$, higher accuracy can be reached because of the decreased importance of quantum jumps at long protocol times, which tend to deteriorate the

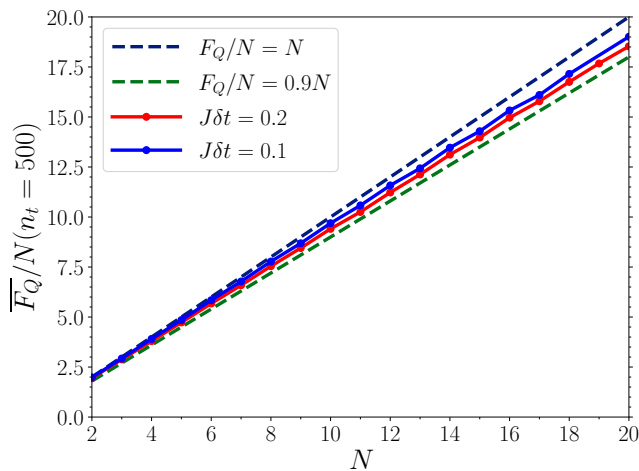


FIG. 4. Scaling of the accuracy of the asymptotic value of the averaged QFI $\overline{F_Q}/N$ vs N for $J\delta t = 0.1$ (blue) and $J\delta t = 0.2$ (red). Results have been averaged over 100 measurement trajectories. Solid lines are guides to the eye only. The upper bound, $\overline{F_Q}/N = N$, is shown as black dashed line, the green dashed line indicates $\overline{F_Q}/N = 0.9N$.

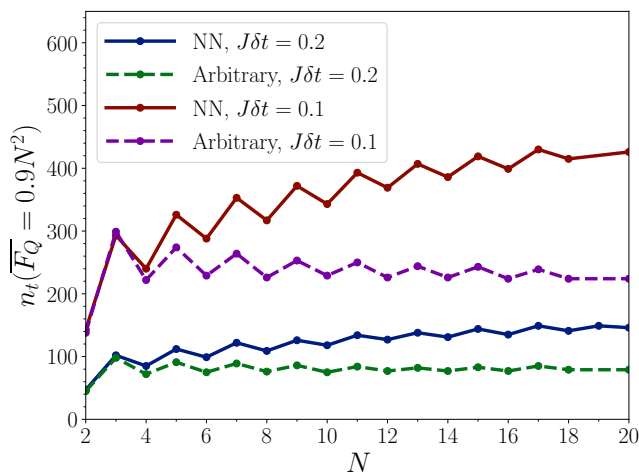


FIG. 5. Scaling of the step number n_t vs N needed for reaching the averaged QFI value $\overline{F_Q} = 0.9N^2$, shown for $J\delta t = 0.1$ and $J\delta t = 0.2$. Averages are over 100 trajectories. Solid and dashed curves are guides to the eye only. We show results for nearest-neighbor detector qubit measurements (solid) as well as allowing for arbitrary detector pair measurements (dashed curves).

QFI momentarily. However, using smaller values for $J\delta t$ comes with longer physical run-times of the protocol.

In Fig. 5, we report the scaling of the number of steps n_t needed for reaching a QFI of $\overline{F_Q}/N^2 = 0.9$, for the same values of $J\delta t$ as in Fig. 4. Here, we also compare to a situation where one allows for Bell pair measurements between arbitrary detector pairs (not only nearest neighbors), which tends to accelerate the protocol. We observe an even-odd effect, in particular

for small N , which originates from the presence of an idle qubit for odd N in our Bell pair measurement scheme, see Fig. 1. Remarkably, the required number of steps n_t increases only very slowly (at most polynomially) with N , suggesting *scalability* of the active steering protocol for large N . This behavior is also corroborated by Fig. 2, where we show the n_t -dependence of $\overline{F_Q}$ for several (large) values of N .

Discussion.—We have proposed an active steering protocol targeting the one-parameter manifold of N -qubit GHZ states (1) with genuine multipartite entanglement by means of weak Bell pair measurements and active feedback. In contrast to fidelity-based cost functions [6], by using the QFI as a cost function, our results suggest that the active steering protocol becomes scalable with increasing system size N . Although it is well known that GHZ states may be generated by projective measurements in shallow circuits [38], our results are relevant for at least two reasons: (i) We clarify similarities and differences between active and passive steering protocols for the case of a target state *manifold*. In passive steering [9, 39], measurement outcomes are discarded. Such protocols are basically equivalent to driven-dissipative systems [40–44] with engineered dissipation, see Refs. [11, 45–59] and corresponding experiments [60–65]. In contrast to the passive steering case, where the initial state uniquely determines the final state within the dark space forming the target manifold [66], we find that under active steering, the quantum state trajectory continues cycling through the target manifold. The initial state then plays no special role, and all phases ϕ in Eq. (1) are reached with equal probability as the protocol evolves. (ii) One may also target highly entangled non-stabilizer state manifolds, for which simpler routes along the lines of Ref. [38] are not available. Under quite general conditions, many highly entangled states, including Eq. (1), cannot be reached by driven-dissipative and/or passive steering [67], while they are accessible to active steering protocols [6]. This task may be achieved, e.g., by adding a non-stabilizerness quantifier term [68, 69] to the cost function, or by stopping the protocol at a suitable value of F_Q before convergence has been reached. Active steering could thus allow for a powerful approach in this case. However, we leave a detailed exploration to future work.

Furthermore, for an experimental implementation, a modified protocol would be highly beneficial where state tracking is not required. It may indeed be possible to formulate such a protocol if weak measurements of all one- and two-body correlations present in the system state $|\Psi\rangle$ can be performed, see also Ref. [11]. In fact, the average cost function change $d\overline{F_Q}$ in Eq. (6) depends only on those correlations.

Finally, given that the manifold achieved by our protocol allows one to overcome classical limits in quantum phase-estimation and to attain the so-called

Heisenberg limit [16–20], it would be interesting to further explore how to use active steering for entanglement-enhanced metrology.

We thank S. Diehl, Y. Gefen, and I. Gornyi for discussions. We acknowledge funding by the Deutsche Forschungsgemeinschaft (DFG, German Research Foundation) under Projektnummer 277101999 - TRR 183 (project B02), and under Germany’s Excellence Strategy - Cluster of Excellence Matter and Light for Quantum Computing (ML4Q) EXC 2004/1 - 390534769.

-
- [1] V. V. Sivak, A. Eickbusch, H. Liu, B. Royer, I. Tsioutsios, and M. H. Devoret, Model-Free Quantum Control with Reinforcement Learning, *Phys. Rev. X* **12**, 011059 (2022).
- [2] Q. Liu, K. Ziegler, D. A. Kessler, and E. Barkai, Driving quantum systems with periodic conditional measurements, *Phys. Rev. Res.* **4**, 023129 (2022).
- [3] A. J. Friedman, O. Hart, and R. Nandkishore, Measurement-Induced Phases of Matter Require Feedback, *PRX Quantum* **4**, 040309 (2023).
- [4] Y. Herasymenko, I. Gornyi, and Y. Gefen, Measurement-Driven Navigation in Many-Body Hilbert Space: Active-Decision Steering, *PRX Quantum* **4**, 020347 (2023).
- [5] V. Ravindranath, Y. Han, Z.-C. Yang, and X. Chen, Entanglement steering in adaptive circuits with feedback, *Phys. Rev. B* **108**, L041103 (2023).
- [6] S. Morales, Y. Gefen, I. Gornyi, A. Zazunov, and R. Egger, Engineering unsteerable quantum states with active feedback, *Phys. Rev. Res.* **6**, 013244 (2024).
- [7] J. Hauser, Y. Li, S. Vijay, and M. P. A. Fisher, Continuous symmetry breaking in adaptive quantum dynamics, *Phys. Rev. B* **109**, 214305 (2024).
- [8] N. Ackermann, S. Morales, A. L. Yeyati, S. Diehl, and R. Egger, **Error threshold in active steering protocols for few-qubit systems** (2024), arXiv:2408.10960 [quant-ph].
- [9] S. Roy, J. T. Chalker, I. V. Gornyi, and Y. Gefen, Measurement-induced steering of quantum systems, *Phys. Rev. Res.* **2**, 033347 (2020).
- [10] R. Uola, A. C. S. Costa, H. C. Nguyen, and O. Gühne, Quantum steering, *Rev. Mod. Phys.* **92**, 015001 (2020).
- [11] H. M. Wiseman and G. J. Milburn, *Quantum measurements and control* (Cambridge University Press, Cambridge, UK, 2010).
- [12] C. W. Helstrom, Quantum detection and estimation theory, *Journal of Statistical Physics* , 231 (1969).
- [13] V. Giovannetti, S. Lloyd, and L. Maccone, Advances in quantum metrology, *Nature photonics* **5**, 222 (2011).
- [14] P. Hyllus, W. Laskowski, R. Krischek, C. Schwemmer, W. Wieczorek, H. Weinfurter, L. Pezzé, and A. Smerzi, Fisher information and multiparticle entanglement, *Phys. Rev. A* **85**, 022321 (2012).
- [15] G. Tóth, Multipartite entanglement and high-precision metrology, *Phys. Rev. A* **85**, 022322 (2012).
- [16] M. G. Paris, Quantum estimation for quantum technology, *International Journal of Quantum Information* **7**, 125 (2009).
- [17] L. Pezzé and A. Smerzi, Entanglement, nonlinear dynamics, and the heisenberg limit, *Phys. Rev. Lett.* **102**, 100401 (2009).
- [18] G. Tóth and I. Apellaniz, Quantum metrology from a quantum information science perspective, *Journal of Physics A: Mathematical and Theoretical* **47**, 424006 (2014).
- [19] L. Pezzé, A. Smerzi, M. K. Oberthaler, R. Schmied, and P. Treutlein, Quantum metrology with nonclassical states of atomic ensembles, *Rev. Mod. Phys.* **90**, 035005 (2018).
- [20] J. Liu, H. Yuan, X.-M. Lu, and X. Wang, Quantum Fisher information matrix and multiparameter estimation, *Journal of Physics A: Mathematical and Theoretical* **53**, 023001 (2019).
- [21] M. A. Nielsen and I. L. Chuang, *Quantum Computation and Quantum Information* (Cambridge University Press, Cambridge, UK, 2000).
- [22] C. Janvier, L. Tosi, L. Bretheau, Ç. Ö. Girit, M. Stern, P. Bertet, P. Joyez, D. Vion, D. Esteve, M. F. Goffman, H. Pothier, and C. Urbina, Coherent manipulation of Andreev states in superconducting atomic contacts, *Science* **349**, 1199 (2015).
- [23] D. Boschi, S. Branca, F. De Martini, L. Hardy, and S. Popescu, Experimental Realization of Teleporting an Unknown Pure Quantum State via Dual Classical and Einstein-Podolsky-Rosen Channels, *Phys. Rev. Lett.* **80**, 1121 (1998).
- [24] J.-W. Pan, D. Bouwmeester, H. Weinfurter, and A. Zeilinger, Experimental Entanglement Swapping: Entangling Photons That Never Interacted, *Phys. Rev. Lett.* **80**, 3891 (1998).
- [25] T. Jennewein, G. Weihs, J.-W. Pan, and A. Zeilinger, Experimental Nonlocality Proof of Quantum Teleportation and Entanglement Swapping, *Phys. Rev. Lett.* **88**, 017903 (2001).
- [26] H. de Riedmatten, I. Marcikic, J. A. W. van Houwelingen, W. Tittel, H. Zbinden, and N. Gisin, Long-distance entanglement swapping with photons from separated sources, *Phys. Rev. A* **71**, 050302 (2005).
- [27] M. Riebe, T. Monz, K. Kim, A. S. Villar, P. Schindler, M. Chwalla, M. Hennrich, and R. Blatt, Deterministic entanglement swapping with an ion-trap quantum computer, *Nature Physics* **4**, 839 (2008).
- [28] R. Kaltenbaek, R. Prevedel, M. Aspelmeyer, and A. Zeilinger, High-fidelity entanglement swapping with fully independent sources, *Phys. Rev. A* **79**, 040302 (2009).
- [29] R. Horodecki, P. Horodecki, M. Horodecki, and K. Horodecki, Quantum entanglement, *Rev. Mod. Phys.* **81**, 865 (2009).
- [30] C.-X. Huang, X.-M. Hu, Y. Guo, C. Zhang, B.-H. Liu, Y.-F. Huang, C.-F. Li, G.-C. Guo, N. Gisin, C. Branciard, and A. Tavakoli, Entanglement Swapping and Quantum Correlations via Symmetric Joint Measurements, *Phys. Rev. Lett.* **129**, 030502 (2022).
- [31] H. P. Breuer and F. Petruccione, *The theory of open quantum systems* (Oxford University Press, Oxford, UK, 2002).
- [32] K. Jacobs and D. A. Steck, A straightforward introduction to continuous quantum measurement, *Contemporary Physics* **47**, 279 (2006).
- [33] J. Zhang, Y. Liu, R.-B. Wu, K. Jacobs, and F. Nori, Quantum feedback: Theory, experiments, and applications, *Physics Reports* **679**, 1 (2017).
- [34] B. Schumacher and M. A. Nielsen, Quantum data processing and error correction, *Physical Review A* **54**,

- 2629 (1996).
- [35] S. Lloyd, Capacity of the noisy quantum channel, *Physical Review A* **55**, 1613 (1997).
- [36] R. Fan, Y. Bao, E. Altman, and A. Vishwanath, Diagnostics of Mixed-State Topological Order and Breakdown of Quantum Memory, *PRX Quantum* **5**, 020343 (2024).
- [37] M. Buchhold, Y. Minoguchi, A. Altland, and S. Diehl, Effective Theory for the Measurement-Induced Phase Transition of Dirac Fermions, *Phys. Rev. X* **11**, 041004 (2021).
- [38] J. F. Kam, H. Kang, C. D. Hill, G. J. Mooney, and L. C. L. Hollenberg, Characterization of entanglement on superconducting quantum computers of up to 414 qubits, *Phys. Rev. Res.* **6**, 033155 (2024).
- [39] E. Medina-Guerra, P. Kumar, I. V. Gornyi, and Y. Gefen, Quantum state engineering by steering in the presence of errors, *Phys. Rev. Res.* **6**, 023159 (2024).
- [40] J. F. Poyatos, J. I. Cirac, and P. Zoller, Quantum Reservoir Engineering with Laser Cooled Trapped Ions, *Phys. Rev. Lett.* **77**, 4728 (1996).
- [41] S. Diehl, A. Micheli, A. Kantian, B. Kraus, H. P. Büchler, and P. Zoller, Quantum states and phases in driven open quantum systems with cold atoms, *Nat. Phys.* **4**, 878 (2008).
- [42] F. Verstraete, M. Wolf, and J. Ignacio Cirac, Quantum computation and quantum-state engineering driven by dissipation, *Nature Physics* **5**, 633 (2009).
- [43] J. T. Barreiro, M. Müller, P. Schindler, D. Nigg, T. Monz, M. Chwalla, M. Hennrich, C. F. Roos, P. Zoller, and R. Blatt, An open-system quantum simulator with trapped ions, *Nature* **470**, 486 (2011).
- [44] H. Krauter, C. A. Muschik, K. Jensen, W. Wasilewski, J. M. Petersen, J. I. Cirac, and E. S. Polzik, Entanglement generated by dissipation and steady state entanglement of two macroscopic objects, *Phys. Rev. Lett.* **107**, 080503 (2011).
- [45] J. P. Paz and W. H. Zurek, Continuous error correction, *Proceedings of the Royal Society of London. Series A: Mathematical, Physical and Engineering Sciences* **454**, 355 (1998).
- [46] J. P. Barnes and W. S. Warren, Automatic Quantum Error Correction, *Phys. Rev. Lett.* **85**, 856 (2000).
- [47] C. Ahn, A. C. Doherty, and A. J. Landahl, Continuous quantum error correction via quantum feedback control, *Phys. Rev. A* **65**, 042301 (2002).
- [48] C. Ahn, H. M. Wiseman, and G. J. Milburn, Quantum error correction for continuously detected errors, *Phys. Rev. A* **67**, 052310 (2003).
- [49] M. Sarovar, C. Ahn, K. Jacobs, and G. J. Milburn, Practical scheme for error control using feedback, *Phys. Rev. A* **69**, 052324 (2004).
- [50] O. Oreshkov and T. A. Brun, Continuous quantum error correction for non-markovian decoherence, *Phys. Rev. A* **76**, 022318 (2007).
- [51] J. Kerckhoff, H. I. Nurdin, D. S. Pavlichin, and H. Mabuchi, Designing Quantum Memories with Embedded Control: Photonic Circuits for Autonomous Quantum Error Correction, *Phys. Rev. Lett.* **105**, 040502 (2010).
- [52] E. Kapit, Hardware-Efficient and Fully Autonomous Quantum Error Correction in Superconducting Circuits, *Phys. Rev. Lett.* **116**, 150501 (2016).
- [53] E. Kapit, Error-Transparent Quantum Gates for Small Logical Qubit Architectures, *Phys. Rev. Lett.* **120**, 050503 (2018).
- [54] M. Gau, R. Egger, A. Zazunov, and Y. Gefen, Driven Dissipative Majorana Dark Spaces, *Phys. Rev. Lett.* **125**, 147701 (2020).
- [55] M. Gau, R. Egger, A. Zazunov, and Y. Gefen, Towards dark space stabilization and manipulation in driven dissipative Majorana platforms, *Phys. Rev. B* **102**, 134501 (2020).
- [56] S. Lieu, R. Belyansky, J. T. Young, R. Lundgren, V. V. Albert, and A. V. Gorshkov, Symmetry Breaking and Error Correction in Open Quantum Systems, *Phys. Rev. Lett.* **125**, 240405 (2020).
- [57] S. Lieu, Y.-J. Liu, and A. V. Gorshkov, Candidate for a Passively Protected Quantum Memory in Two Dimensions, *Phys. Rev. Lett.* **133**, 030601 (2024).
- [58] O. Shtanko, Y.-J. Liu, S. Lieu, A. V. Gorshkov, and V. V. Albert, *Bounds on Autonomous Quantum Error Correction* (2023), arXiv:2308.16233 [quant-ph].
- [59] L. B. Kristensen, M. Kjaergaard, C. K. Andersen, and N. T. Zinner, Hybrid quantum error correction in qubit architectures, *Phys. Rev. A* **108**, 022403 (2023).
- [60] Z. Leghtas, U. Vool, S. Shankar, M. Hatridge, S. M. Girvin, M. H. Devoret, and M. Mirrahimi, Stabilizing a Bell state of two superconducting qubits by dissipation engineering, *Phys. Rev. A* **88**, 023849 (2013).
- [61] Z. K. Mineev, S. O. Mundhada, S. Shankar, P. Reinhold, R. Gutiérrez-Jáuregui, R. J. Schoelkopf, M. Mirrahimi, H. J. Carmichael, and M. H. Devoret, To catch and reverse a quantum jump mid-flight, *Nature* **570**, 200 (2019).
- [62] P. Campagne-Ibarcq, A. Eickbusch, S. Touzard, E. Zalys-Geller, N. E. Frattini, V. V. Sivak, P. Reinhold, S. Puri, S. Shankar, R. J. Schoelkopf, L. Frunzio, M. Mirrahimi, and M. H. Devoret, Quantum error correction of a qubit encoded in grid states of an oscillator, *Nature* **584**, 368 (2020).
- [63] J. M. Gertler, B. Baker, J. Li, S. Shirol, J. Koch, and C. Wang, Protecting a bosonic qubit with autonomous quantum error correction, *Nature* **590**, 243 (2021).
- [64] W. P. Livingston, M. S. Blok, E. Flurin, J. Dressel, A. N. Jordan, and I. Siddiqi, Experimental demonstration of continuous quantum error correction, *Nature Communications* **13**, 2307 (2022).
- [65] D. Lachance-Quirion, M.-A. Lemonde, J. O. Simoneau, L. St-Jean, P. Lemieux, S. Turcotte, W. Wright, A. Lacroix, J. Fréchet-Viens, R. Shillito, F. Hopfmueller, M. Tremblay, N. E. Frattini, J. Camirand Lemyre, and P. St-Jean, Autonomous Quantum Error Correction of Gottesman-Kitaev-Preskill States, *Phys. Rev. Lett.* **132**, 150607 (2024).
- [66] P. Zanardi and L. Campos Venuti, Coherent Quantum Dynamics in Steady-State Manifolds of Strongly Dissipative Systems, *Phys. Rev. Lett.* **113**, 240406 (2014).
- [67] F. Ticozzi and L. Viola, Stabilizing entangled states with quasi-local quantum dynamical semigroups, *Philosophical Transactions of the Royal Society A: Mathematical, Physical and Engineering Sciences* **370**, 5259 (2012).
- [68] A. Ahmadi and E. Greplova, Quantifying non-stabilizerness via information scrambling, *SciPost Phys.* **16**, 043 (2024).
- [69] P. S. Tarabunga, M. Frau, T. Haug, E. Tirrito,

and L. Piroli, [A nonstabilizerness monotone from stabilizerness asymmetry](#) (2024), [arXiv:2411.05766 \[quant-ph\]](#).